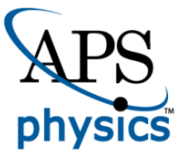

Optomechanical Quantum Information Processing with Photons and Phonons

K. Stannigel, P. Komar, S. J. M. Habraken, S. D. Bennett, M. D. Lukin, P. Zoller, and P. Rabl

Phys. Rev. Lett. **109**, 013603 — Published 6 July 2012

DOI: 10.1103/PhysRevLett.109.013603

Optomechanical quantum information processing with photons and phonons

K. Stannigel[1,2], P. Komar[3], S. J. M. Habraken[1], S. D. Bennett[3], M. D. Lukin[3], P. Zoller[1,2], P. Rabl[1]
[1] *Institute for Quantum Optics and Quantum Information, 6020 Innsbruck, Austria*
[2] *Institute for Theoretical Physics, University of Innsbruck, 6020 Innsbruck, Austria and*
[3] *Physics Department, Harvard University, Cambridge, Massachusetts 02138, USA*

We describe how strong resonant interactions in multimode optomechanical systems can be used to induce controlled nonlinear couplings between single photons and phonons. Combined with linear mapping schemes between photons and phonons, these techniques provide a universal building block for various classical and quantum information processing applications. Our approach is especially suited for nano-optomechanical devices, where strong optomechanical interactions on a single photon level are within experimental reach.

PACS numbers: 42.50.Wk, 03.67.Hk, 07.10.Cm

Optomechanics describes the radiation pressure interaction between an optical cavity mode and the motion of a macroscopic mechanical object, as it appears, for example, in a Fabry-Perot cavity with a moveable mirror [1]. First demonstrations of optomechanical (OM) laser cooling [2] have recently attracted significant interest and led to tremendous progress in the development of new fabrication methods and experimental techniques for controlling OM interactions at the quantum level. Apart from ground state cooling [3, 4], this includes the demonstration of slow light [5, 6], and the coherent interconversion of optical and mechanical excitations [7, 8]. These achievements pave the way for a new type of quantum light-matter interface and give rise to interesting perspectives for novel OM based quantum technologies. As a solid state approach, such an all OM platform would benefit directly from advanced nanofabrication and scalable integrated photonic circuit techniques. At the same time long mechanical lifetimes comparable to atomic systems allow to combine optical nonlinearities with a stationary quantum memory for light.

In this work we study strong OM coupling effects in *multimode* OM systems (OMS) and describe how resonant or near-resonant interactions in this setting allow us to exploit the intrinsic nonlinearity of radiation pressure in an optimal way. Our approach is based on the resonant exchange of photons between two optical modes mediated by a single phonon. This resonance induces much stronger nonlinearities than achievable in single mode OMS, where nonlinear effects are suppressed by a large mechanical frequency [9–12]. Consequently, multimode OMS provide a promising route for accessing the single photon strong coupling regime, where the coupling g_0 as well as the mechanical frequency ω_m exceeds the cavity decay rate κ [11]. This regime is within reach of state of the art nanoscale OM devices [4, 13, 15, 16] or analogous cold atom OMS [17, 18] and here we discuss how strong OM interactions in a multimode setup can be used to generate single photons and to perform controlled gate operations between photonic or mechanical qubits. Combined with very recently developed photon-phonon interfaces and quantum memories based on linearized OM couplings [7, 8, 19], our results provide a basis for efficient OM classical and quantum information processing with applications ranging from photon transistors to quantum repeaters and networks.

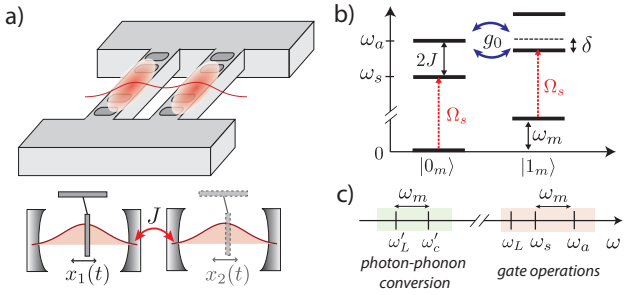

FIG. 1. (color online) a) Setup of two tunnel-coupled OM crystal cavities (see Ref. [4, 13] for more details). b) Level diagram showing the lowest mechanical and optical excitations in a two mode OMS. Resonant coupling ($\delta = 0$) occurs when the tunnel splitting $2J$ between the optical modes is comparable to the mechanical frequency ω_m. c) Different sets of strongly and weakly coupled optical modes and control laser fields can be used for nonlinear interactions ($\omega_s, \omega_a, \omega_L$) and purely linear photon storage and retrieval operations (ω_c', ω_L').

Model. We consider a setup of two tunnel-coupled OMS [19–23] as schematically shown in Fig. 1, focusing on the OM crystal design [4, 13] as a specific example. Each OMS $i = 1, 2$ is represented by an optical mode of frequency ω_c and a bosonic operator c_i, which is coupled via optical gradient forces to the motion of an isolated mechanical mode b_i with vibrational frequency ω_m^i. The Hamiltonian for this system is ($\hbar = 1$)

$$H = \sum_{i=1,2} \omega_m^i b_i^\dagger b_i + \omega_c c_i^\dagger c_i + g_0 c_i^\dagger c_i (b_i + b_i^\dagger) - J(c_1^\dagger c_2 + c_1 c_2^\dagger) + \sum_{i=1,2} \Omega_i (c_i e^{i\omega_L t} + \text{H.c.}), \quad (1)$$

where J is the tunneling amplitude between the optical modes and g_0 denotes the single photon OM cou-

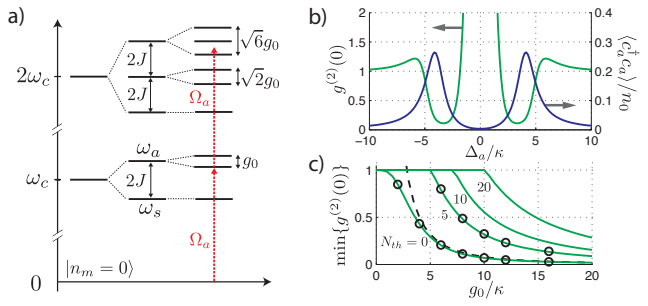

FIG. 2. (color online) a) Energy level diagram of a resonantly coupled OMS, $\delta = 2J - \omega_m = 0$, and for a single mechanical mode in the ground state. b) Excitation spectrum and $g^{(2)}(0)$ for a weak coherent field exciting the c_a mode, where $g_0/\kappa = 8$ and $n_0 = \Omega_a^2/\kappa^2$. c) Minimal value of $g^{(2)}(0)$ as a function of the OM coupling strength g_0 and different values of N_{th}. The analytical results (solid lines) given in the text are in good agreement with exact numerics (circles). The dashed line shows the asymptotic scaling $\sim 8\kappa^2/g_0^2$ at zero temperature.

pling. The Ω_i are the local amplitudes of an external control laser field of frequency ω_L. Below we also consider an additional set of cavity modes and driving fields with frequencies ω_c' and ω_L', respectively. As indicated in Fig. 1(c) we assume these modes to be separated in frequency and used for cooling the mechanical mode [24, 25], and linear photon storage and retrieval operations [7, 8, 26, 27] only.

Apart from the coherent dynamics described by Eq. (1), we include dissipation through cavity decay and mechanical damping and model the evolution of the system density operator ρ by a master equation (ME)

$$\dot\rho = -i[H,\rho] + \sum_i \kappa\mathcal{D}[c_i]\rho + \mathcal{L}_\gamma\rho, \qquad (2)$$

where $\mathcal{D}[c]\rho = 2c\rho c^\dagger - \{c^\dagger c,\rho\}_+$, and $\mathcal{L}_\gamma = \sum_i \frac{\gamma}{2}(N_{th}+1)\mathcal{D}[b_i] + \frac{\gamma}{2}N_{th}\mathcal{D}[b_i^\dagger]$. Here κ is the optical field decay rate, $\gamma = \omega_m/Q$ the mechanical damping rate for a quality factor Q and $N_{th} = (e^{\hbar\omega_m/k_BT}-1)^{-1}$ the mechanical equilibrium occupation number for temperature T. Below we identify $\Gamma_m = \frac{\gamma}{2}(3N_{th}+\frac{1}{2})$ as the characteristic decoherence rate for mechanical qubit states [28].

Resonant strong-coupling optomechanics. In the following we are interested in the strong coupling regime $\omega_m, g_0 \gg \kappa, \Gamma_m$, and our main goal is to show how the multi-mode OMS described by Eq. (1) can be used for implementing controlled interactions between qubits encoded in photonic or phononic degrees of freedom. To illustrate this we first consider a single mechanical resonator, $b \equiv b_1$, $\omega_m \equiv \omega_m^1$. We introduce symmetric and antisymmetric optical modes $c_{s,a} = (c_1 \pm c_2)/\sqrt{2}$ with eigenfrequencies $\omega_{s,a}$ split by $2J$. Further, we assume that $\omega_m \sim 2J \gg g_0, \kappa, |\delta|$, where $\delta = 2J - \omega_m$ (see Fig. 1(b)). This condition can be achieved in nano-scale OMS where $\omega_m \sim$ GHz [4, 13, 15, 16] and a matching tunnel splitting can be designed by appropriately adjusting the spacing between the cavities [13, 20]. In this regime we can make a rotating wave approximation with respect to the large frequency scale $\omega_m \sim 2J$ and after changing into a frame rotating with ω_L we obtain [20]

$$\begin{aligned} H =& -\Delta_s c_s^\dagger c_s - \Delta_a c_a^\dagger c_a + \omega_m b^\dagger b \\ &+ \frac{g_0}{2}(c_a c_s^\dagger b^\dagger + c_a^\dagger c_s b) + H_\Omega(t). \end{aligned} \qquad (3)$$

Here $\Delta_{s,a} = \omega_L - \omega_{s,a}$ are the detunings of the driving field from the c_s and c_a mode respectively, and $H_\Omega(t) = \sum_{\eta=s,a}(\Omega_\eta(t)c_\eta + \text{H.c.})$ accounts for the external driving fields with slowly varying amplitudes $\Omega_{s,a}(t) = (\Omega_1(t) \pm \Omega_2(t))/\sqrt{2}$.

The two-mode OM coupling in Eq. (3) describes photon transitions between the energetically higher mode c_a to the lower mode c_s, while simultaneously absorbing or emitting a phonon. For $(\Delta_s - \Delta_a - \omega_m) = \delta = 0$, this leads to a resonant interaction between states $|n_a, n_s, n_m\rangle$ and $|n_a - 1, n_s + 1, n_m + 1\rangle$, where n_a, n_s and n_m label the occupation numbers of the two optical modes and the mechanical mode, respectively. In analogy to atomic cavity QED [29], the nonlinear scaling of the corresponding transition amplitudes $\frac{g_0}{2}\sqrt{n_a(n_s+1)(n_m+1)}$ results in an anharmonic level diagram as shown in Fig. 2(a). If g_0 exceeds the cavity linewidth κ, one and two photon transitions can be spectrally resolved, indicating the onset of strong single photon nonlinearities.

An OM single photon source. As a first application of the nonlinear OM interaction we discuss the use of the OMS as a single photon source, which is characterized by a vanishing equal time two-photon correlation function $g^{(2)}(0)$. In Fig. 2(b) we plot the excitation spectrum $\langle c_a^\dagger c_a\rangle$ and $g^{(2)}(0) = \langle c_a^\dagger c_a^\dagger c_a c_a\rangle/\langle c_a^\dagger c_a\rangle^2$, for the case where only the c_a mode is weakly driven. Around the single photon resonances $\Delta_a = \pm g_0/2$ we observe strong anti-bunching $g^{(2)}(0) < 1$ as a clear signature of non-classical photon statistics. To quantify this effect we assume that $\Gamma_m \ll \kappa$, which allows us to treat subspaces connected to different $|n_m\rangle$ separately. For weak driving fields $\Omega_a \ll \kappa$ the system dynamics can then be restricted to the six states $|0_a, 0_s, n_m\rangle, |1_a, 0_s, n_m\rangle, |0_a, 1_s, n_m + 1\rangle, |2_a, 0_s, n_m\rangle, |1_a, 1_s, n_m+1\rangle, |0_a, 2_s, n_m+2\rangle$ and we calculate the relevant occupation probabilities $p_{1,0,n_m}$ and $p_{2,0,n_m}$ to leading order in Ω_a [30]. We obtain

$$p_{1,0,n} = \left|\frac{4\Omega_a d}{X_n}\right|^2, \qquad p_{2,0,n} = 8\left|\frac{\Omega_a^2(8d^2 - g_0^2)}{(X_n(2X_n - g_0^2))}\right|^2, \qquad (4)$$

where $d = \Delta_a - i\kappa$ and $X_n = d^2 - g_0^2(n+1)$. By taking the appropriate thermal averages, $\langle n_a\rangle = \sum_n \zeta_n p_{1,0,n}$ and $g^{(2)}(0) = 2\sum_n \zeta_n p_{2,0,n}/\langle n_a\rangle^2$, where $\zeta_n = (1 - e^{-\beta\hbar\omega_m})e^{-\beta\hbar\omega_m n}$ and $\beta^{-1} = k_BT$, the two photon correlation function can be evaluated for arbitrary temperatures T.

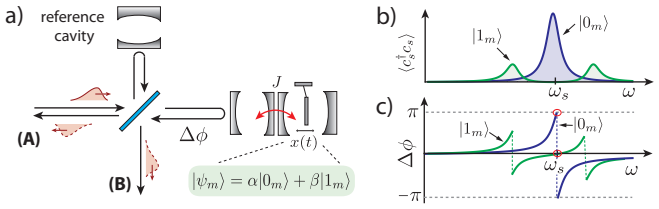

FIG. 3. (color online) A single phonon - single photon transistor. a) An incoming photon in port (A) passes through the interferometric setup and leaves through port (A) or (B), depending on the phase shift $\Delta\phi$ acquired upon reflection from the two mode OMS. b), c) For a mechanical system in state $|0_m\rangle$, the OMS exhibits a single resonance at ω_s ($\Delta\phi = \pi$), while for state $|1_m\rangle$ the resonance splits by $g_0 \gg \kappa$ and the photon does not enter the cavity ($\Delta\phi = 0$).

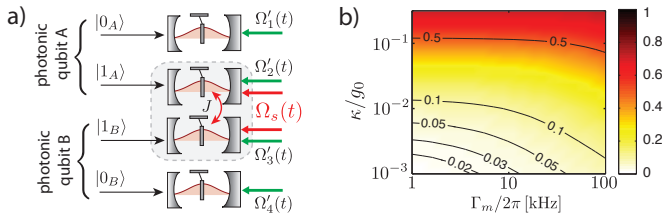

FIG. 4. (color online) a) OM quantum memory, where 'path-encoded' photonic qubits are stored in long-lived mechanical states using tunable linearized OM interactions $\sim \Omega_i'(t)$. Deterministic gate operation between stationary qubits are implemented by a controlled phonon-phonon interaction $\sim \Omega_s(t)$ as described in the text. b) The total error ϵ_g for implementing a controlled phase gate between two phononic qubits is minimized with respect to Δ_s and plotted as a function of κ and Γ_m (see text). The parameters for this plot are $g_0/(2\pi) = 50$ MHz, $\gamma/(2\pi) = 4$ kHz, $\alpha = 1$ and $g_0/\delta = 1/3$.

In Fig. 2(c) we plot the minimal value of $g^{(2)}(0)$ as a function of the coupling strength g_0 and for different N_{th}. As the OM coupling increases we find that for $T = 0$ the minimum of the correlation functions scales as $\min_{\Delta_a}\{g^{(2)}(0)\} \simeq 8\kappa^2/g_0^2$. This demonstrates an improved scaling over off-resonant photon blockade effects in single mode OMS, where for large ω_m only a small reduction $g^{(2)}(0) \simeq 1 - g_0^2/(\kappa\omega_m)$ can be obtained [11]. Since the positions of the single and two-photon resonances depend explicitly on the mechanical state $|n_m\rangle$, finite temperature degrades the quality of the single photon source. Nevertheless, with increasing coupling strength the anti-bunching effect becomes surprisingly robust and when combined with cooling cycles to achieve $\langle n_m\rangle \sim 1$ [4], allows the operation of OM single photon sources even at environmental temperatures of a few Kelvin.

Single-phonon single-photon transistor. Given the ability to generate single photons, Fig. 3 illustrates a basic scheme for using the same resonant OMS to implement a two qubit gate [31]. First, we assume that the state of a control photon is mapped onto a mechanical superposition state $\alpha|0_m\rangle + \beta|1_m\rangle$. This can be achieved with conventional cooling followed by photon-phonon conversion techniques using linearized OM interactions with an auxiliary mode ω_c' (see Fig. 1(c). Next, a single target photon of central frequency $\sim \omega_s$ is sent through the interferometric setup as described in Fig. 3. If the mechanical mode is in the state $|0_m\rangle$ the incoming photon couples to a single resonant state $|0_a, 1_s, 0_m\rangle$ (see Fig. 1(b), such that it enters the cavity and picks up a phase before being reflected. Instead, if the mechanical resonator is in the state $|1_m\rangle$ the resonant coupling between $|0_a, 1_s, 1_m\rangle$ and $|1_a, 0_s, 0_m\rangle$ splits the cavity resonance and for $g_0 > \kappa$ the photon is reflected without a phase shift. Under ideal conditions the final result is an entangled state

$$|\psi\rangle = \alpha|0_m, 1_A, 0_B\rangle + \beta|1_m, 0_A, 1_B\rangle, \qquad (5)$$

where A and B are the two ports of the interferometer. This state can be converted back into an entangled state between the initial control and the target photon.

By assuming that the storage and the retrieval of the control photon can be achieved with high fidelity, the error for producing the entangled state (5) with $\alpha = \beta = 1/\sqrt{2}$ is approximately given by

$$\epsilon \approx \frac{4\kappa^2}{g_0^2} + \frac{1}{(\tau_p\kappa)^2} + \tau_p\Gamma_m, \qquad (6)$$

where τ_p is the duration of the single photon pulse. The individual contributions in Eq. (6) arise from an imperfect photon reflection, the finite spectral width of the photon pulse, and mechanical decoherence, respectively. The minimal error is achieved for $\tau_p^{-1} \approx \sqrt[3]{\kappa^2\Gamma_m}$ where we obtain $\epsilon \approx \max\{4\kappa^2/g_0^2, \sqrt[3]{\Gamma_m^2/\kappa^2}\}$. Assuming an OM crystal device with $\omega_m/(2\pi) = 4$ GHz and $Q = 10^5$ as discussed in Ref. [4], but with an improved OM coupling $g_0/(2\pi) = 50$ MHz and a lower decay rate $\kappa/(2\pi) = 5$ MHz, we obtain gate errors $\epsilon \approx 0.1$ for environmental temperatures around $T \approx 100$ mK.

Phonon-phonon interactions. Finally, we consider the possibility to perform a controlled gate operation between two qubits stored in long-lived mechanical modes. Our approach is depicted in Fig. 4(a), and combines the long coherence times of OM quantum memory [7, 8, 26, 27] with the practical utility of exploiting interactions between stationary phononic qubits. We focus on the limit $\Gamma_m \ll \kappa$, and assume that optical (e.g. 'path encoded') qubits are first mapped onto long-lived states $|0_m\rangle$ and $|1_m\rangle$ of two or more mechanical modes. The OM coupling is then employed to generate nonlinear interactions between the phonons only.

We consider nonlinear interactions between two mechanical modes b_1 and b_2 described by Eq. (1), detuned from resonance such that $g_0 < |(2J - \omega_m^i)|$ and direct

transitions between photons and phonons are suppressed. To obtain the effective phonon-phonon interactions, we first diagonalize H to second order in $\xi_i = g_0/(2J - \omega_m^i)$ with the transformation $H \rightarrow e^{iS} H e^{-iS}$, where $S = \frac{i}{2}(c_s^\dagger c_a(\xi_1 b_1^\dagger - \xi_2 b_2^\dagger) - \text{H.c.})$. This yields $H = H_0 + H_g + H_\Omega(t)$, where $H_0 = -\Delta_s c_s^\dagger c_s - \Delta_a c_a^\dagger c_a + \sum_i \omega_m^i b_i^\dagger b_i$,

$$H_g = \frac{g_0}{4}\left[(c_s^\dagger c_s + 1) c_a^\dagger c_a (\xi_1 + \xi_2) + (c_a^\dagger c_a - c_s^\dagger c_s)\mathcal{N}_b\right], \quad (7)$$

and we have neglected small corrections to the driving Hamiltonian $H_\Omega(t)$. The phonon operator in Eq. (7) is given by $\mathcal{N}_b = \xi_1 b_1^\dagger b_1 + \xi_2 b_2^\dagger b_2 - (\xi_1 + \xi_2)(b_1^\dagger b_2 + b_2^\dagger b_1)/2$. For simplicity we focus on symmetric detuning, $\omega_m^{1,2} = 2J \mp \delta$, where $\mathcal{N}_b = \frac{g_0}{\delta}(b_1^\dagger b_1 - b_2^\dagger b_2)$. The transformation also modifies the dissipative terms in the Eq. (2); most importantly we find an optically-induced decay channel for the mechanical modes, $\mathcal{L}_\gamma \rightarrow \mathcal{L}_\gamma + \kappa g_0^2/(4\delta^2)\mathcal{D}[c_s(b_1 + b_2)]$.

We assume that only the c_s mode is weakly driven by a slowly-varying control field $\Omega_s(t)$. In this case the c_a mode remains unpopulated and we neglect it. Next we shift the driven mode, $c_s \rightarrow \alpha + c_s$ by the classical amplitude α, yielding an effective ME for c_s, b_1 and b_2. Finally, we adiabatically eliminate the c_s mode, valid in the limit $|\alpha| \sim \mathcal{O}(1)$ and $(g_0^2|\alpha|/4\delta) \ll |\Delta_s + i\kappa|$, to obtain an effective master equation for the mechanical modes [32],

$$\begin{aligned}\dot{\rho}_m = &-i[H_m + \Lambda(b_1^\dagger b_1 - b_2^\dagger b_2)^2, \rho_m] + \mathcal{L}_\gamma \rho_m \\ &+ \Gamma_\phi \mathcal{D}[(b_1^\dagger b_1 - b_2^\dagger b_2)]\rho_m + \frac{\gamma'}{2}\sum_i \mathcal{D}[b_i]\rho_m.\end{aligned} \quad (8)$$

Here $\gamma' = \kappa|\alpha|^2 g_0^2/(2\delta^2)$ and the phonon-phonon interaction and the phonon dephasing rate are given by

$$\Lambda = \frac{g_0^4|\alpha|^2\Delta_s}{16\delta^2(\Delta_s^2 + \kappa^2)}, \qquad \Gamma_\phi = \frac{g_0^4|\alpha|^2\kappa}{16\delta^2(\Delta_s^2 + \kappa^2)}. \quad (9)$$

The effective Hamiltonian in Eq. (8) describes a phonon nonlinearity with a tunable strength $\Lambda(t) \sim |\alpha(t)|^2$. The relevant cross-coupling is given by

$$H_{\text{int}} \simeq 2\Lambda b_1^\dagger b_1 b_2^\dagger b_2, \quad (10)$$

and when acting for a time $t_g = \pi/(2\Lambda)$ this Hamiltonian implements a controlled-phase gate between two qubits encoded in states $|0_m\rangle$ and $|1_m\rangle$. During this time, phonons experience intrinsic and optically-induced decoherence as seen in Eq. (8). In Fig. 4 we plot the resulting gate error $\epsilon_g = 1 - \langle\psi_0|\rho_m(t_g)|\psi_0\rangle$ for an initial state $|\psi_0\rangle = \frac{1}{2}(|0_m\rangle + |1_m\rangle)^{\otimes 2}$ optimized with respect to Δ_s. Using the total decoherence rate of this state, $\Gamma_{\text{decoh}} = 2\Gamma_m + \Gamma_\phi + \gamma'/2$, we find that $\epsilon_g \propto \Gamma_{\text{decoh}}/\Lambda$ is minimized for $|\Delta_s| \simeq g_0/2$ where $\epsilon_g \propto 4(\kappa/g_0)$. While this scaling with g_0 is weaker than for a gate based on photon reflection (see Eq. (6)), the ability to perform a gate between stationary qubits represents an important advantage of this approach.

Conclusions. We have described single photon and single phonon nonlinear effects in strongly coupled multimode OMS. We have shown how induced nonlinearities on or near resonance can be used for controlled quantum gate operations between flying optical or stationary phononic qubits. Our results provide a realistic route towards the quantum nonlinear regime of OMS, and a framework for future OM information processing applications.

Acknowledgments. The authors thank D. Chang, O. Painter and M. Aspelmeyer for stimulating discussion. This work was supported by NSF, CUA, DARPA, the Packard Foundation, the EU project AQUTE and the Austrian Science Fund (FWF) through SFB FOQUS and the START grant Y 591-N16.

Note added. During completion of this project we became aware of a related work by M. Ludwig *et al.* [33].

[1] T. J. Kippenberg and K. J. Vahala, Science **321**, 1172 (2008); F. Marquardt and S. M. Girvin, Physics **2**, 40 (2009); M. Aspelmeyer and K. Schwab, New J. Phys. **10**, 095001 (2008).
[2] C. H. Metzger and K. Karrai, Nature **432**, 1002 (2004). S. Gigan *et al.*, Nature **444**, 67 (2006). O. Arcizet *et al.*, Nature **444**, 71 (2006). D. Kleckner and D. Bouwmeester, Nature **444**, 75 (2006). T. Corbitt *et al.*, Phys. Rev. Lett. **99**, 160801 (2007). J. D. Thompson *et al.*, Nature **452**, 72 (2008); A. Schliesser *et al.*, Nature Physics **4**, 415 (2008); D. J. Wilson *et al.*, Phys. Rev. Lett. **103**, 207204 (2009).
[3] J. D. Teufel *et al.*, Nature **471**, 204 (2011).
[4] J. Chan *et al.*, Nature **478**, 89 (2011).
[5] S. Weis *et al.*, Science **330**, 1520 (2010).
[6] A.H. Safavi-Naeini *et al.*, Nature **472**, 69 (2011).
[7] V. Fiore *et al.*, Phys. Rev. Lett. **107**, 133601 (2011).
[8] E. Verhagen *et al.*, Nature **482**, 63 (2012).
[9] W. Marshall *et al.*, Phys. Rev. Lett. **91**, 130401 (2003).
[10] M. Ludwig *et al.*, New J. Phys. **10**, 095013 (2008).
[11] P. Rabl, Phys. Rev. Lett. **107**, 063601 (2011).
[12] A. Nunnenkamp *et al.*, Phys. Rev. Lett. **107**, 063602 (2011).
[13] M. Eichenfield *et al.*, Nature **462**, 78 (2009).
[14] A. H. Safavi-Naeini *et al.* , Phys. Rev. Lett. **108**, 033602 (2012).
[15] T. Carmon and K. Vahala, Phys. Rev. Lett., **98** 123901, (2007).
[16] L. Ding *et al.*, Appl. Phys. Lett. **98**, 113108 (2011).
[17] S. Gupta *et al.*, Phys. Rev. Lett. **99**, 213601 (2007).
[18] F. Brennecke *et al.*, Science **322**, 235 (2008).
[19] A. H. Safavi-Naeini and O. Painter, New J. Phys. **13**, 013017 (2011).
[20] I. S. Grudinin *et al.*, Phys. Rev. Lett. **104**, 083901 (2010).
[21] J. M. Dobrindt and T. J. Kippenberg, Phys. Rev. Lett. **104**, 033901 (2010).
[22] H. Miao *et al.*, Phys. Rev. Lett. **103**, 100402 (2009).
[23] H. K. Cheung and C. K. Law, Phys. Rev. A **84**, 023812 (2011).

[24] F. Marquardt *et al.*, Phys. Rev. Lett. **99**, 093902 (2007).
[25] I. Wilson-Rae *et al.*, Phys. Rev. Lett. **99**, 093901 (2007).
[26] J. Zhang *et al.*, Phys. Rev. A **68**, 013808 (2003).
[27] U. Akram *et al.*, N. J. Phys. **12**, 083030 (2010).
[28] Γ_m corresponds to the initial decoherence rate of a phonon superposition $(|0_m\rangle + |1_m\rangle)/\sqrt{2}$.
[29] J. M. Raimond *et al.*, Rev. Mod. Phys. **73** 565 (2001).
[30] H. J. Carmichael *et al.*, Opt. Comm. **82** 73 (1991).
[31] L.-M. Duan and H. J. Kimble, Phys. Rev. Lett. **92**, 127902 (2004).
[32] See Supplemental Material for more details on the derivation of ME (8).
[33] M. Ludwig, A. H. Safavi-Naeini, O. Painter, F. Marquardt, *Optomechanical photon detection and enhanced dispersive phonon readout*, arXiv:1202.0532.